The Crystal Structure of *Pichia pastoris* Lysyl Oxidase†

Anthony P. Duff,‡ Aina E. Cohen,§ Paul J. Ellis,§ Jason A. Kuchar,⊥,# David B. Langley,‡ Eric M. Shepard,⊥ David M. Dooley,*,⊥ Hans C. Freeman,*,‡ and J. Mitchell Guss*,‡

School of Molecular and Microbial Biosciences, University of Sydney, Sydney, N.S.W. 2006, Australia, Stanford Synchrotron Radiation Laboratory, 2575 Sandhill Road, Menlo Park, California 94025 USA, and Department of Chemistry and Biochemistry, Montana State University, Bozeman, Montana 59717 USA

Received July 28, 2003; Revised Manuscript Received October 7, 2003

ABSTRACT: *Pichia pastoris* lysyl oxidase (PPLO) is unique among the structurally characterized copper amine oxidases in being able to oxidize the side chain of lysine residues in polypeptides. Remarkably, the yeast PPLO is nearly as effective in oxidizing a mammalian tropoelastin substrate as is a true mammalian lysyl oxidase isolated from bovine aorta. Thus, PPLO is functionally related to the copper-containing lysyl oxidases despite the lack of any significant sequence similarity with these enzymes. The structure of PPLO has been determined at 1.65 Å resolution. PPLO is a homodimer in which each subunit contains a Type II copper atom and a topaquinone cofactor (TPQ) formed by the posttranslational modification of a tyrosine residue. While PPLO has tertiary and quaternary topologies similar to those found in other quinone-containing copper amine oxidases, its active site is substantially more exposed and accessible. The structural elements that are responsible for the accessibility of the active site are identified and discussed.

Amine oxidases catalyze the oxidative deamination of primary, secondary, and tertiary amines to the corresponding aldehydes, with the subsequent reduction of O_2 to H_2O_2 (as illustrated for a primary amine):

$$RCH_2NH_3^+ + O_2 + H_2O \rightarrow RCHO + NH_4^+ + H_2O_2$$

The amine oxidases found in mammals fall into two groups: quinone-containing copper amine oxidases (CuAOs)[1] and flavin-dependent monoamine oxidases (MAOs). MAOs are found exclusively in the outer mitochondrial membrane of virtually all cell types (*1*). These enzymes degrade primary, secondary, and tertiary amines and are involved in the oxidation of several neurotransmitters. MAOs are believed to function either through a single electron-transfer mechanism or through a concerted covalent catalysis mechanism, both involving the FAD cofactor (*1*).

Quinone-containing CuAOs, on the other hand, appear to be involved exclusively in the oxidative deamination of primary amines. These enzymes can be subdivided into two classes based on the type of quinone cofactor present in the active site: 2,4,5-trihydroxyphenylalanine quinone (TPQ) or lysyl tyrosylquinone (LTQ) (Figure 1). Enzymes of the latter class, known as lysyl oxidases, have long been known to be associated with connective tissue formation through catalyzing the crucial deamination of the side-chain of peptidyl lysine that initiates cross-linking of lysine residues in collagen and elastin (*2*, *3*). While biogenesis of the LTQ cofactor has yet to be examined, TPQ biogenesis has been extensively studied, inter alia using multiple trapped crystal structures (*4*). The conversion of a Tyr residue to TPQ requires only apo-unprocessed enzyme, copper, and molecular oxygen (*5*−*9*).

Catalysis by CuAOs proceeds through a ping-pong mechanism (as illustrated in Figure 2 of Wilmot et al. (*10*)). The key step is the conversion of the initial quinoneimine "substrate Schiff base" to a quinolaldimine "product Schiff base", facilitated by proton abstraction from the α carbon of substrate by an absolutely conserved aspartate acting as a general base (*11*, *12*). Hydrolysis causes release of aldehyde product, giving a Cu(II)-aminoresorcinol in equilibrium with Cu(I)-semiquinone, which subsequently reacts with dioxygen to produce H_2O_2 and an iminoquinone. The iminoquinone is then hydrolyzed, liberating NH_4^+, and returning the cofactor to its resting state (*12*). An alternative reaction pathway, where copper reduction is not required for cofactor reoxidation, has also been proposed (*13*, *14*). The trapping and characterization of a number of reaction intermediates by the Leeds group (*11*) have provided some structural support for these proposals. While the detailed catalytic steps

† This work is supported by the following grants: Australian Research Council Grant DP0208320 to H.C.F. and J.M.G.; National Institutes of Health (NIH) Grant GM27659 to D.M.D.; the SSRL Structural Molecular Biology Program is supported by the Department of Energy, Office of Biological and Environmental Research and by the NIH, National Center for Research Resources, Biotechnology Program and the National Institute of General Medical Sciences.

* To whom correspondence should be addressed. (D.M.D.) Tel: +1 406 994 4371. Fax: +1 406 994 7989. E-mail: dmdooley@montana.edu. (H.C.F.) Tel: +61 (0)2 9351 4405. Fax: +61 (0)2 9351 4726. E-mail: freemanh@chem.usyd.edu.au. (J.M.G.) Tel: +61 (0)2 9351 4302. Fax: +61 (0)2 9351 4726. E-mail: m.guss@mmb.usyd.edu.au.

‡ University of Sydney.

§ Stanford Synchrotron Radiation Laboratory

⊥ Montana State University

Present address: Department of Pharmacology and Physiology, University of Rochester, Rochester, NY 14642, USA.

[1] Abbreviations: AGAO, *Arthrobacter globiformis* amine oxidase; CuAO, copper-containing amine oxidase; DPI, diffraction precision indicator; ECAO, *Escherichia coli* amine oxidase; HPAO, *Hansenula polymorpha* amine oxidase; LTQ, lysyl tyrosyl quinone; MAO, monoamine oxidase; PPLO, *Pichia pastoris* lysyl oxidase; rmsd, root-mean-square difference; PSAO, *Pisum sativum* (pea seedling) amine oxidase; TPQ, 2,4,5-trihydroxyphenylalanine quinone.

10.1021/bi035338v CCC: $25.00
Published on Web 12/02/2003

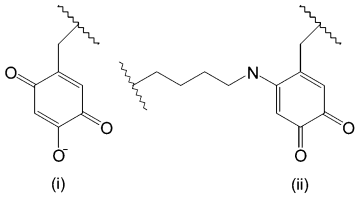

FIGURE 1: Modified amino acid residues that act as cofactors in CuAOs. Linkages to the protein are shown as wavy lines. (i) 2,4,5-trihydroxyphenylalanine quinone, TPQ, found in most CuAOs, and derived from a Tyr residue and (ii) lysyl tyrosyl quinone, LTQ, found in mammalian lysyl oxidases and formed from linked Tyr and Lys residues.

for the mammalian LTQ containing lysyl oxidase enzymes have yet to be determined, the similarity of LTQ and TPQ and the presence of copper in both types of CuAO suggest that the catalytic mechanisms are similar (*3*).

TPQ-containing CuAOs are distributed widely in nature and have been purified from mammals, plants, and microorganisms. They are involved in the oxidation of many short- to long-chain aliphatic mono- and diamines, including several aromatic amines (*12*, *15*). In microorganisms, they frequently have a nutritional role in the utilization of primary amines as the sole source of nitrogen or carbon (*12*). The role of amine oxidases in higher organisms is not as clear. In plants, it is hypothesized that CuAOs are involved in cell wall biosynthesis (*16*). Further, plant amine oxidases are involved in processes of development and senescence, wound healing, the reduction of the concentration of toxic amines, and the biosynthesis of alkaloids and hormones (*16*, *17*). In mammals, amine oxidases appear to be tissue specific and are thought to have functions in detoxification, cell growth, signaling, adhesion (*18*, *19*), and apoptosis (*15*, *16*).

The three-dimensional structures for CuAOs from *Escherichia coli* (ECAO) (*20*), *Pisum sativum* (PSAO) (*21*), *Arthrobacter globiformis* (AGAO) (*12*), and *Hansenula polymorpha* (HPAO) (*22*) have provided a rational basis for experiments and speculation concerning the enzyme mechanism and the biogenesis of the TPQ cofactor. The four CuAOs have the same overall architecture and topology. All have a single active site containing one type II copper ion and the TPQ cofactor per subunit (*23*−*25*). The active sites are located in the large core domain, a β-sandwich, which contains approximately 400 residues (domain D4). N-terminal to the core are two other domains with similar α/β topologies (D2 and D3). ECAO alone contains an additional N-terminal stalk domain (D1) (*20*). The additional domain in ECAO led to the structure being described as mushroom shaped, with D2, D3, and D4 representing the cap and the N-terminal D1 as the stalk (*20*). A highly unusual feature of the structures is a large solvent-filled cavity or "lake" in the interior of the dimer, between the two D4 domains. The copper site in each subunit backs onto the lake, with the TPQ cofactor lying on the distal side of the copper atom. A long and narrow channel connects the TPQ to the external solvent (*12*). Two unusual β-hairpin arms extend from the central domain of one subunit along the surface of the other subunit. Residues at the end of one arm form part of the entrance to the active-site channel. The number and types of residues in the β-hairpin arms are variable, as indicated by published CuAO structures and amino acid sequences (*12*, *22*). The TPQ cofactor has been observed in two distinct conformations in the various structures. In one conformation, it is coordinated directly to the copper atom. Since it was originally observed in ECAO under conditions in which the enzyme was shown to be inactive, this conformation has been described as "inactive" (*11*). Other structural data have subsequently suggested that the position of the TPQ may be dynamic, and its location is now described as either "on-copper" or "off-copper" (*24*). It appears that substrates can interact with the TPQ to form the enzyme−substrate complex only when the TPQ is in the "off-copper" position.

The two classes of CuAO having TPQ and LTQ, respectively, at the active site are unrelated at the sequence level. Classifying newly discovered CuAOs can be difficult, since their most prominent shared property is an ability to oxidize primary amines. In the search for yeasts that can live with small organic amines as their sole source of nitrogen, researchers identified several CuAOs with methylamine or benzylamine as the preferred substrate in *Candida boidinii* and in *Pichia pastoris* (*26*). It was originally hoped that a purified enzyme of this type could be used as an analytical agent for the quantitation of amines, but a competing reaction in which the enzyme oxidizes lysine residues in peptides made this impossible (*26*). The "lysyl oxidase-like" activity of the *P. pastoris* enzyme was later fully characterized, and it was shown that lysine and lysine peptides are among the preferred substrates for the enzyme in vitro (*27*). This enzyme, termed *P. pastoris* lysyl oxidase (PPLO), was cloned and overexpressed (*28*). The quinone cofactor was unequivocally identified as TPQ by chemical isolation and Raman spectroscopy (*29*). Thus, PPLO is a TPQ-containing CuAO with the ability to oxidize peptidyl lysine side chains. In this respect, it resembles the LTQ-containing mammalian amine oxidases. Further, while many CuAOs display broad substrate specificity, PPLO has by far the broadest substrate range among known CuAOs, oxidizing a large number of short- to long-chain aliphatic amines, including several aromatic amine derivatives (*28*). This paper describes the high-resolution crystal structure of PPLO. Analysis of the structure contributes to our understanding of the unique ability of PPLO, in contrast with other TPQ containing CuAOs, to include lysine and lysine peptides among the primary amines that it can oxidize. As a demonstration of this ability, we show that PPLO displays catalytic activity toward tropoelastin (the un-cross-linked form of elastin) at a rate comparable with that of a true mammalian lysyl oxidase.

METHODS

Crystallization, X-ray Data Collection, and Processing. The protein was expressed and purified as described previously (*28*, *29*). The crystallization, data collection and preliminary X-ray analysis for crystals described as "form 1" and "form 2" have been published (*30*). Diffraction data for the structure analysis described in this work, corresponding to "form 2", were recorded from a single crystal ($0.2 \times 0.1 \times 0.1$ mm^3) at beamline 9−1 of the Stanford Synchrotron Radiation Laboratory. The outermost shell of data at 1.65 Å resolution has a significant signal, $\langle I/\sigma(I)\rangle$, of 2.6. The statistics for the data used in the structure solution and refinement are given in Table 1.

Structure Solution. The structure of PPLO was solved by molecular replacement, with the program AMoRe (*31*). A

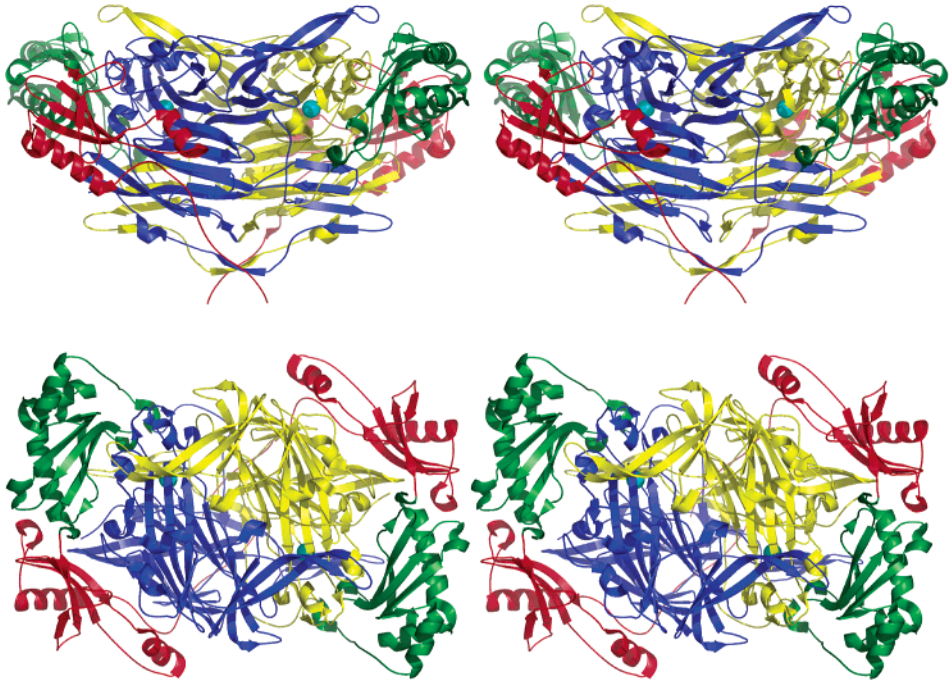

FIGURE 2: Stereoviews of PPLO in two orientations. In the upper view, the 2-fold axis of molecular symmetry lies vertically in the plane of the paper. In the lower view, the molecule is rotated so that the viewer is looking along the 2-fold axis. The ribbon representation is colored to highlight the domain structure: D2, red; D3, green; D4 from subunit A, blue; D4 from subunit B, yellow. The Cu atom in each D4 domain is shown as a cyan sphere. Figures 2, 4, and 6 were prepared with program PyMOL (*44*).

Table 1: Crystallographic Data and Structure Refinement Statistics for *Pichia pastoris* Lysyl Oxidase

space group	*C*2
unit cell dimensions	$a = 248.4$, $b = 121.1$, $c = 151.8$ Å, $\beta = 124.6°$
resolution (Å)	24.6−1.65
redundancy	2.8 (2.6)[a]
$I/\sigma(I)$	13.7 (2.4)
completeness (%)	94.7 (90.7)
R_{merge}[b]	0.06 (0.42)
overall *B* value (Wilson plot) (Å^2)	16.5
number of non-hydrogen atoms refined	28,232
number of reflections	419,014 (28,231)
R_{cryst}[c]	0.161 (0.240)
R_{free} (5% of data)	0.187 (0.271)
R_{total} (final cycle)	0.160 (0.230)
DPI[d] (Å)	0.09
Ramachandran plot	
residues in most favored regions (%)	87.8
residues in allowed regions (%)	12.2
rmsd from standard geometry	
bond lengths (Å)	0.01
bond angles (°)	1.5
average *B* values (Å^2)	
protein atoms	16.4
solvent	27.1

[a] Numbers in parentheses refer to the highest resolution shell, 1.68−1.65 Å. Complete statistics for the data collection have been published (*30*). [b] $R_{merge} = \Sigma|I_h - \langle I_h\rangle|\Sigma\langle I_h\rangle$. [c] *R* values $= \Sigma|F_{obs} - F_{calc}|\Sigma F_{obs}$. R_{total} is the *R* value following the final cycles of refinement, in which all the data were used. [d] DPI is the diffraction precision indicator (*45*).

reasonable value of the Matthews' coefficient (*32*) predicts the presence of two dimers (four subunits) in the asymmetric unit. It was assumed that pairs of subunits would dimerize with 2-fold symmetry similar to that observed in other CuAO structures. The search model was derived from the ECAO structure (PDB entry: 1OAC (*20*)), which had the highest-ranking pairwise alignment with PPLO in a blast search (*33*). The sequence of PPLO matches residues 216−715 of ECAO with 25% identity and 41% similarity. The homologous residues comprise more than half of D2, and all of D3 and D4. Two search models were used to locate the two dimers in the asymmetric unit of PPLO. One consisted of a dimer of ECAO including all atoms corresponding to the aligned regions of the sequence, and the other was this structure converted into a poly-serine peptide. Rotation functions were calculated at resolutions from 3 to 5 Å, in 0.5 Å steps with both models. The top two unique solutions for the rotation function subsequently proved to be the correct solutions for the two dimers. A translation function to locate the first dimer was calculated for the top 41 rotation function solutions. The top solution was used to fix the first dimer in a translation search for the second. The translation search for the second dimer used the remaining top 40 rotation function solutions and gave a clear result with an *R* value of 0.58 for data to 4 Å resolution. The positions of the two dimers were optimized as rigid bodies using the FITFUN step of AMoRe, resulting in a residual $R = 0.55$ for the data to 3.0 Å resolution. Visual inspection of this solution indicated that the molecules packed in the crystal without overlap.

Structure Refinement. The resulting model was first refined with CNS (*34*) using simulated annealing to remove some of the model bias. Strong 4-fold noncrystallographic restraints were used. At this stage, electron density maps calculated with data from 7 to 3 Å were poor and yielded little additional information. The residuals were $R = 0.524$ and $R_{free} = 0.55$. Side chains were added to the model in default conformations, using O (*35*) and faithfully following the blast sequence homology alignment. Further electron-density maps were calculated: (i) with real-space averaged σA weights, (ii) with solvent flattening and 4-fold reciprocal space

averaging using DM (*36*), and (iii) using a procedure in ARPwARP (*37*) to add oxygen atoms into regions of positive difference electron density and remove atoms in weak electron density. Although the individual maps were still poor, using a combination of maps made it possible to remove parts of the structure that were modeled incorrectly. This resulted in small decreases in both R and R_{free}. More importantly, it led to significant improvements in the electron-density maps. At its minimum, the model consisted of four monomers of only 344 residues, 71 without side chains, a total of 12688 atoms, representing 45% of the final refined model. The values of R and R_{free} were 0.47 and 0.49, respectively. Many cycles of manual model fitting using O (*35*), and refinement eventually allowed the completion of the polypeptide chain. From this point onward, refinement was carried out with REFMAC5 (*38*). The strong noncrystallographic symmetry restraints applied during the early stages of the refinement were removed in the final cycles.

Once the model for the polypeptide was essentially complete, water molecules were added, using PEAKMAX (*39*) and WATPEAK (*39*). Solvent sites were required to have a well-resolved difference electron-density peak greater than 4σ, and a position permitting the formation of hydrogen bonds with reasonable stereochemistry. Each solvent site was examined manually during the refinement and after the final cycle to ensure that it met the stated criteria. Partially occupied solvent sites belonging to alternative solvent networks were allowed only if they were associated with $2F_O-F_C$ density greater than 1.5σ. Electron-density maps clearly indicated the presence of *N*-linked carbohydrate (*N*-acetylglucosamine) at all five putative glycosylation sites, and these were added to the model. The carbohydrate content expected for the five observed glycosylation sites per subunit is consistent with the difference between the molecular mass determined by SDS−PAGE (112 kDa) and that calculated from the amino acid sequence (90 kDa for residues 1−787). Regions of the polypeptide with multiple conformations were included only if they were confirmed using omit maps.

Some regions of difference electron density contained relatively strong positive features, which could not easily be identified. Where possible, these were interpreted as networks of partially occupied solvent and were modeled accordingly. The copper atoms were associated with the largest positive peaks in a difference electron-density map, having the same locations in the molecule as in other CuAO structures. Two other large peaks in each subunit were modeled as Ca^{2+} ions on the basis of their peak heights and stereochemistries. The identity of the Ca^{2+} ions was confirmed by analyzing the anomalous signal as a function of X-ray energy at SSRL beamline 9-2. Sulfate ions were included on a similar basis. In each subunit, one SO_4^{2-} ion appeared to be disordered as indicated by the shape of residual difference electron density. Attempts to refine these SO_4^{2-} ions (numbered 811, 821, 831, and 841) were not successful, and they are included in the deposited coordinates with zero occupancy. The TPQ residue was included only in the final stages of the refinement to ensure minimum bias in its orientation. The coordinates and structure factors have been deposited with the Protein Data Bank as entry PDB ID 1N9E.

Measurement of Lysyl Oxidase Activity. The activity of two genuine lysyl oxidases and five CuAOs against tropoelastin was measured using the ^3H-release assay (detecting the appearance of ^3H in water from the assay mixture), as previously described by Kagan and co-workers (*40*). Recombinant, radiolabeled tropoelastin was prepared by slight modifications of the method as described by Kagan and co-workers (*41*); the recombinant *E. coli* strain expressing human tropoelastin was generously provided by Dr. Herb Kagan (Boston University School of Medicine). 4,5-[^3H]-lysine was purchased from Amersham Pharmacia Biotech and incorporated into the tropoelastin as previously described. Bovine aorta lysyl oxidase was purified by the method of Kagan and Cai (*42*).

Substrate Modeling. A hexapeptide substrate was modeled into the active site of PPLO to visualize the restrictions on substrate size and orientation. The hexapeptide, HKHYDV, was chosen on the basis of having the highest k_{cat}/K_M reported for a substrate of PPLO (*27*). The peptide was placed in a tight β-turn-β motif using a segment of the PPLO structure (residues A477−A501) and then mutating the residues using program O. The single Lys residue was placed at the apex of the turn. The hexapeptide was manually maneuvered into the funnel, avoiding steric clashes, until the lysine N^{ζ} atom overlapped the O5 of TPQ using program O. The energy of the complex structure was then minimized with CNS.

Miscellaneous Calculations. The PPLO structure was superposed on the known CuAO structures using an initial orientation generated by the least-squares routines in O. Volumes of inland lakes were calculated using VOIDOO Version 971120/3.1.2 (*43*). Cavity entrances were blocked by mutating surface side chains to larger amino acids. Buried surface areas were calculated using AREAIMOL version 4.2 (*39*). Default parameters were used unless otherwise stated.

RESULTS

The Crystallographic Result. The structure of PPLO (Figure 2) has been refined at 1.65 Å resolution. The final residuals are $R = 0.160$ and $R_{free} = 0.187$. Data were collected from a single crystal of "form 2" as previously reported (*30*). Within the limits of precision, the two homodimers in the asymmetric unit are identical with the exception of a few surface side-chain orientations. Each subunit comprises residues 41−775 of the published sequence. Residues 1−40 of the DNA-derived sequence were lost from the *N*-terminus before final purification, as confirmed by N-terminal sequencing. The 12 C-terminal residues, 776−787, are presumed to be disordered. The active site of each subunit includes a Cu(II) atom coordinated by the side chains of three histidine residues and the TPQ cofactor. Each subunit also contains two tightly bound Ca^{2+} ions, five glycosylation sites at which at least one carbohydrate (NAG) residue is resolved, and six SO_4^{2-} ions. There are 3981 solvent sites per asymmetric unit.

Summary of the Structure. In overall architecture, PPLO is similar to the other CuAOs. Like AGAO, HPAO, and PSAO, but unlike ECAO, it does not have a known D1 domain. However, it is possible that residues 1−40 of the gene product, which were missing from the protein used for the structure analysis, constitute a D1 domain in vivo. Residues 41−55 form an isolated N-terminal strand, and are analogous to the D1−D2 linker in ECAO. Residues 56−169 form domain D2. Residues 170−305 form domain D3.

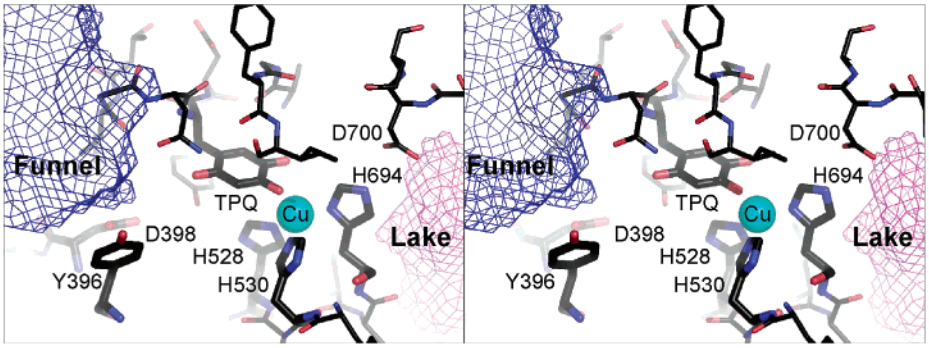

FIGURE 3: Stereoview of the active site of PPLO showing the relative locations of the Cu atom, the ligands to the copper, His 528, His 530, His 694, and the TPQ. The funnel (blue) and the lake (red) are shown as solvent accessible surfaces.

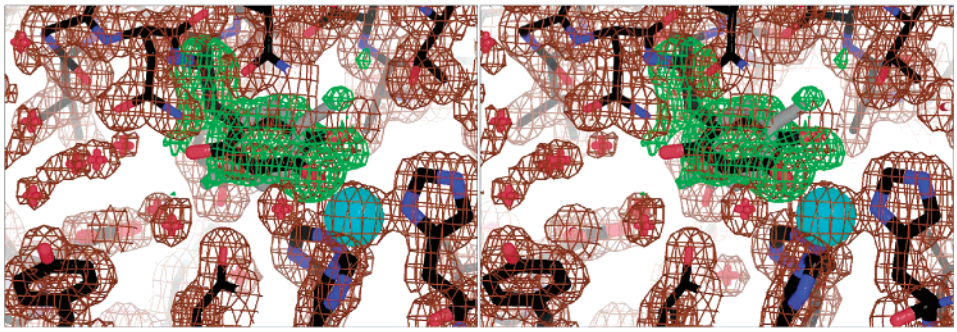

FIGURE 4: Stereoviews of electron density difference maps at the PPLO active site. $2F_O-F_C$ electron-density, brown, contoured at 0.9σ and "omit" electron-density, green, contoured at 3σ. The "omit" density was calculated with values of F_C to which the atoms of TPQ did not contribute. Some of the solvent sites are associated with lower levels of electron-density and may be occupied only partially.

Residues 306−331 link D3 to D4, as an isolated, extended loop wrapped around the symmetry-related D4 domain. Residues 332−750 form the domain D4. The copper site is buried deep in D4. This domain includes protrusions, which we have named the "upper arm" (residues 545−578) and the "lower arm" (residues 450−463 comprising "hairpin 1", and residues 732−750 comprising "hairpin 2"), respectively. These arms embrace the symmetry-related domain D4 of the dimer. The C-terminal strand (residues 751−775) wraps around the enzyme, contacting the D4 core and the D1−D2 linker. The C-terminal and N-terminal strands are linked by a disulfide bond from Cys 756 to Cys 45. In the dimer, the D4 domains and the D3−D4 linkers form a single core domain containing 890 residues.

Significant Differences from Other Copper Amine Oxidases. There are a number of functionally important differences between the structure of PPLO and the published structures of other CuAOs. The most dramatic of these is an expansion of the previously observed narrow channel to the active site into a broad funnel. There are additional residues at a number of positions in domain D2 (residues 83−93, 131−134, 148−152, 156−165), domain D3 (residues 191−194, 200−202, 215−218, 271−292) and domain D4 (residues 733−752). The effects of these additional residues are (i) to create a new helix (residues 271−292), which interacts with residues in the catalytic domain D4 along the rim of a funnel to the active site, and (ii) to create a new β-hairpin (residues 732−750). The new hairpin interacts with one of the β-hairpin arms previously identified in all CuAO structures, forming a 4-stranded β-sheet, which is packed tightly against the surface of the catalytic domain of the other subunit. At the end of the new hairpin, a sequence of acidic residues, DDETEE, contributes to the electrostatic properties of the entrance to the active site. Notwithstanding these changes at the surface and the subunit interface, the core of domain D4, including the active-site region, is conserved.

The formation of the new hairpin loop places Cys 756 near the C-terminus close to Cys 45 near the N-terminus, leading to the formation of an intra-subunit disulfide bond. The disulfide bonds in the two subunits of the dimer are related in such a way that the polypeptide chains have the topology of two links in a chain. This topology depends on the intertwining of the two polypeptide chains prior to disulfide bond formation.

Active Site and Its Environment. The active site (Figure 3) comprises a copper atom coordinated by the side chains of three histidines (His 528, His 530, and His 694) and by O4 of the TPQ (residue 478). Thus, TPQ is in the "on-copper" rather than the "off-copper" position. There is no evidence one of the histidine residues that coordinates the copper is disordered as observed in AGAO (*12*). However, the main chain at residues 525−526 clearly exists in two conformations. In one of these, the peptide carbonyl oxygen atom makes a hydrogen bond with $N^{\delta 1}$ of the Cu ligand His 528. This histidine residue nevertheless is well resolved in a single conformation. The electron density for TPQ is consistent with the presence of a minor conformer (not included in the final model but shown in Figure 4) resulting from rotation about the $C^{\beta}-C^{\gamma}$ bond. The TPQ is "on-copper" in both conformations, and its Cu-binding O4 atom remains in the same position. In one of the two orientations of TPQ, its O5 atom can form a hydrogen bond with a conserved residue, Tyr 384, but this interaction is clearly not strong enough to restrain the TPQ. The position of Asp 398 in the active site (Figure 3) is consistent with the proposed role of this residue as the totally conserved catalytic

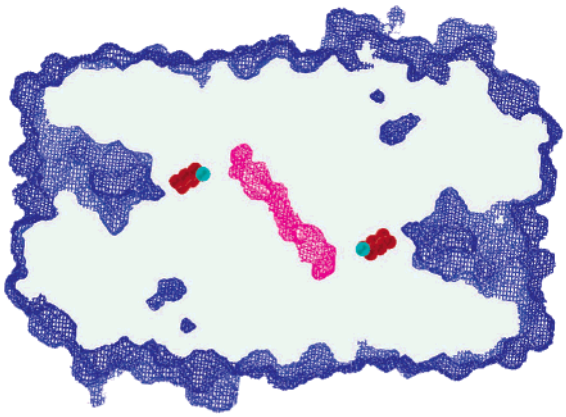

FIGURE 5: Cross section through the PPLO dimer represented as a solvent-accessible surface. The interior of the protein is shaded gray. The external surface of the protein is blue and that of the internal lake is magenta. Wide funnels give access to the active sites in the two subunits. Balls represent the Cu atoms (cyan) and TPQ residues (red).

base (Asp 298 in AGAO) (*11*, *12*). Tyr 396 occupies the position assigned in other amine oxidase structures to the "active-site gate". It lies between the "open" and "closed" conformations observed in other CuAO structures, but closer to the "open" position.

Hydrogen-bond networks connect the active site to ordered solvent regions on the funnel side as well as the inland lake side. On the funnel side, the water network extends to oxygen atoms of the TPQ. On the side of the inland lake, the water network (the edge of the lake) extends to Asp 700, which is hydrogen-bonded to a copper ligand, His 694. Thr 474, which is part of the conserved active-site motif TXXNYD, is hydrogen-bonded to a conserved acidic residue, Asp 479, which in turn is hydrogen-bonded to His 453 on the β-hairpin arm extending from the other subunit. This arrangement of Thr 474, Asp 479, and His 453 is conserved in all structurally characterized CuAOs.

It has been suggested that in HPAO there is a dioxygen-binding site between three residues corresponding to Tyr 480, Ala 498, and Thr 704 in PPLO (*22*). In the present structure, the close proximity of the TPQ when it is in the "on-copper" position would prevent the accommodation of O_2 at this site. However, we cannot eliminate the possibility that an O_2 molecule can be accommodated at the proposed site when the TPQ residue is in its "off-copper" conformation.

Subunit Interfaces and an Inland Lake. The interface between the two subunits of the dimer buries 8700 Å^2 of solvent-accessible area per subunit. This large buried surface area is consistent with the observation that PPLO and other amine oxidases are dimers in solution. The dimer contact consists of an annular interface between the D4 domains of the two subunits and extended surfaces resulting from the embedding of the arms of one subunit in the surface of the other. The embracing arms contribute 42% of the buried area.

As a result of the dimer formation, the subunits enclose an "inland lake" of 1000 Å^3 (Figure 5). (The volume of the lake is calculated for a model in which connections with the external solvent are blocked.) Comparable lake volumes in other CuAOs are 550 Å^3 in ECAO, 900 Å^3 in AGAO, 1200 Å^3 in HPAO, and 1450 Å^3 in PSAO. In PPLO, the inland lake is connected to the external solvent by a channel along the noncrystallographic 2-fold dimer axis, between residues Glu 589 in the two subunits. The orientation of the carboxylate groups of these two residues is not well determined. The distance between corresponding C$^\gamma$ atoms is ~7 Å. Unobstructed movements of the Glu 589 side chains could widen this gap. Evidence that the channel permits the entry of small ions is provided by the presence of two ordered SO_4^{2-} ions in the lake. We conclude that the connection between the external solvent and the inland lake offers a pathway for the transport of small molecules and ions, e.g., substrate O_2, product H_2O_2, and product NH_4^+, as others have similarly conjectured (*22*).

A Unique Funnel Defines Substrate Specificity. In contrast to all other structurally characterized copper amine oxidases, PPLO does not require substrates to negotiate a narrow channel to gain access to the active site. Instead, the active site lies at the base of such a wide-mouthed funnel that it is effectively exposed to the solvent. The funnel is deep with a wide bottom and steep walls (Figure 6). The protein surface around the top of the funnel is irregular. There are three turret-like formations on the rim (Figure 6). The highest peak is 24 Å above the base of the funnel, and the minimum height of troughs between the turrets is 12 Å. At this height, the funnel has an approximately circular cross-section and a diameter of 10 Å.

The wall of the funnel has contributions from residues 84−89 of domain D2; residues 173−177, 179−184, 186−188, 191 and its attached carbohydrate, 207−216, 234−238, and 240−243 of domain D3; residues 355, 390, 396, 400−401, 405−407, 428−431, 433, 435, 474−477, 503, and 660−661 of domain D4; residues 769−775 at the C-terminus (and possibly the unobserved residues 776−787); residues 453−457, and 737−742 of the four-stranded beta sheet composed of the loops from the other subunit. The base of the funnel is composed almost exclusively of residues from D4.

The increased size of the funnel compared with the channels to the active sites of other amine oxidases is a consequence of movements of 4−6 Å of residues in D3. For example, in relation to ECAO, there are concerted movements of a helix, residues 175−189 in PPLO (188−202 in ECAO) and a β-strand residues 209−216 in PPLO (219−226 in ECAO). These movements are accommodated by a similar movement of a β-hairpin, residues 248−269 in PPLO (262−281 in ECAO). In several instances, these shifts are augmented by PPLO having less bulky residues than ECAO (for example, Ser 179 and Gly 211 in PPLO compared with the corresponding residues Phe 192 and Ile 221 in ECAO). Further, the portion of the funnel wall contributed by the arm from the neighboring subunit (hairpin 1 of the lower arm) is shorter than in any other amine oxidase so far characterized. The enlarged opening of the funnel is buttressed by a new helix (residues 276−287) and by the insertion of a strand of polypeptide from the C-terminus (residues 771−775).

The distribution of charged side-chains on the walls of the funnel is electrostatically unbalanced (Figure 6b). A group of positively charged residues (Arg 176, Arg 335, Arg 406, Arg 435, and Arg 772) lie on one side, and a group of negatively charged residues (Glu 238, Asp 240, and Glu 242) lie on the other. The base of the funnel is composed of polar and aromatic residues. If the TPQ residue is modeled in the "off-copper" position by analogy with the conformation observed in an ECAO−inhibitor complex (PDB entry 1SPU

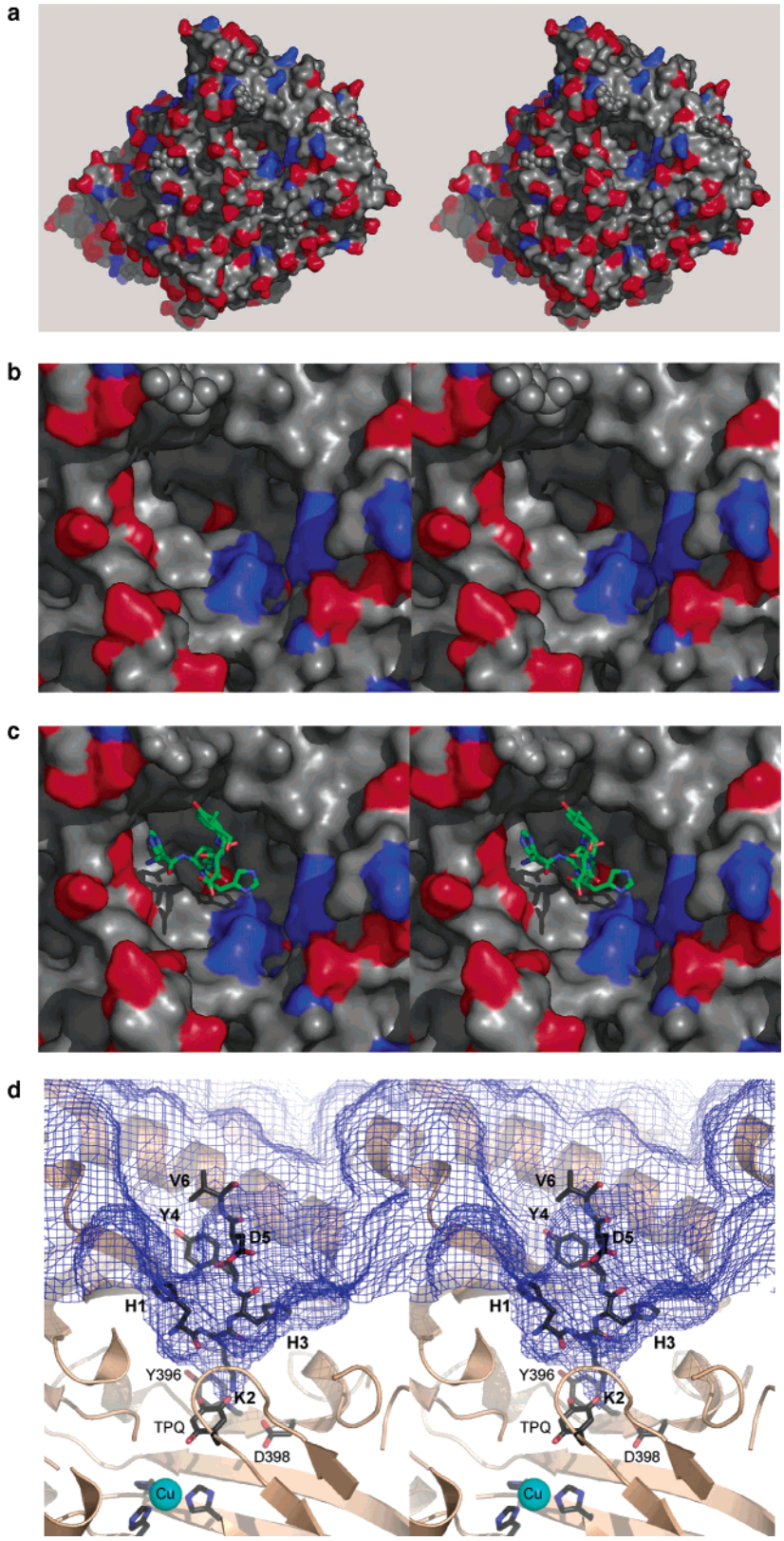

FIGURE 6: Stereoviews showing the active-site funnel in a single subunit of PPLO. The protein atoms are shown as a molecular surface (positively charged residues, blue; negatively charged residues, red; other residues, gray). Attached carbohydrate residues are the only features drawn as CPK atoms. (a) Surface of the subunit looking down into the active-site funnel. (b) Closer view of the funnel, showing the "lumpy" nature of the funnel rim. (c) Model of a hexapeptide (HKHYDV) substrate docked into the active site. (d) Alternative view of the model hexapeptide substrate in the active-site funnel, showing the interaction with the TPQ cofactor.

(*11*)), the surrounding residues are Asn 477, Gly 476, Ile 475, Tyr 396, Tyr 401. These residues are conserved among the structurally characterized CuAOs. In addition, a loop protruding from the rim of the funnel (the turret with the highest peak) has a sequence of negatively charged residues (D_{738} $DETEE_{743}$).

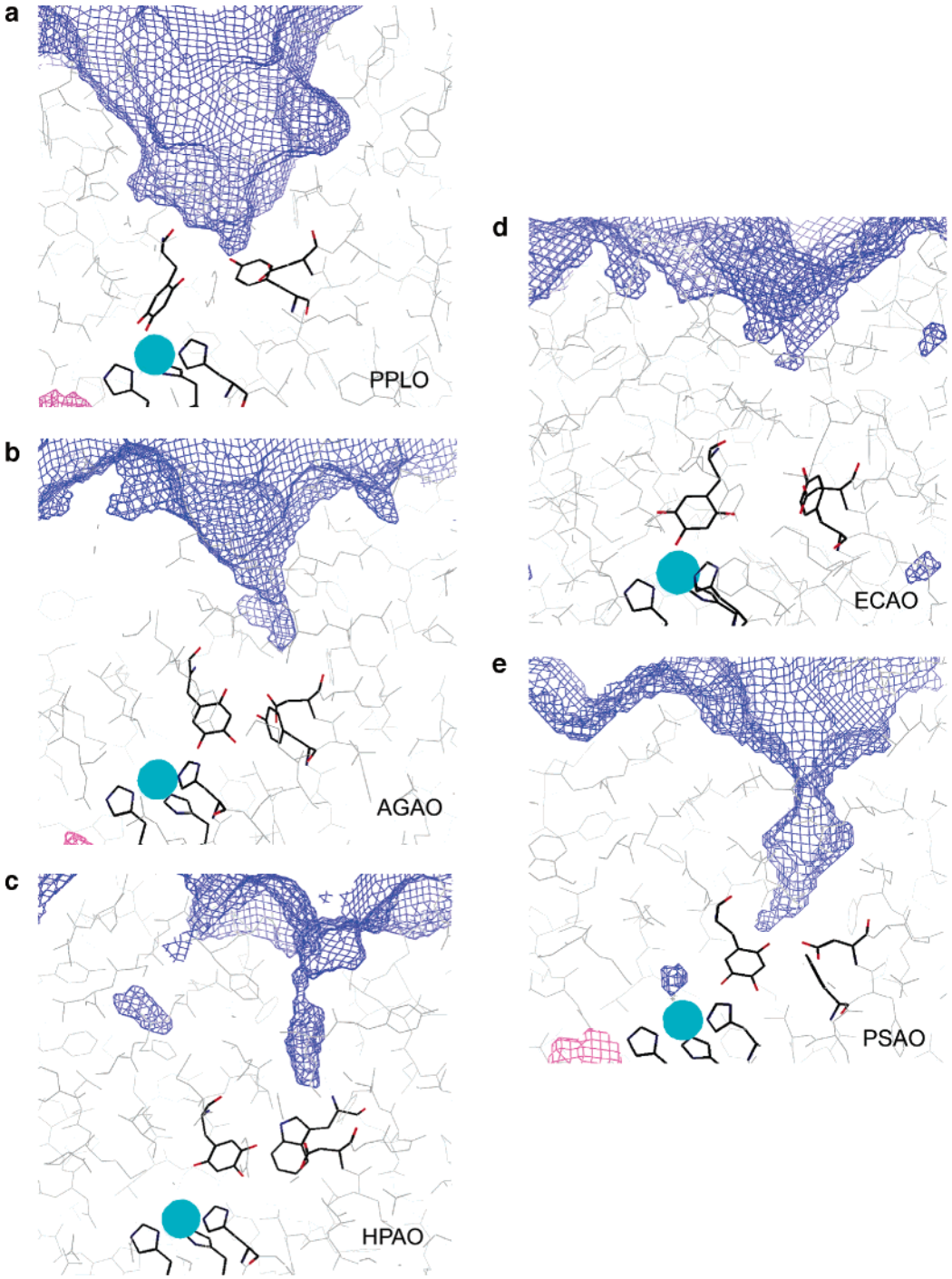

FIGURE 7: Views of the active-site funnels in the known CuAO structures. (a) PPLO, (b) AGAO, (c) HPAO, (d) ECAO, and (e) PSAO. The surface of each funnel is shown as a blue mesh. The residues in the interior of a protein are drawn in gray, the copper atom is a cyan sphere, and the copper ligands, TPQ, active-site base, and "gate" residues are drawn with heavy lines. A small portion of the interior lake is seen, colored magenta, at the bottom of some figures.

DISCUSSION

The funnel leading to the active site in PPLO is substantially more accessible than in any other structurally characterized amine oxidase (Figure 7). The O2 atom of the TPQ is visible from the solvent even when TPQ is in its "on-copper" position. Atoms O4 and O5 would be more accessible when TPQ is in the "off-copper" position. In other CuAOs, a gating role has been assigned to an aromatic residue close to the TPQ (*12*). The corresponding residue in PPLO is Tyr 396. It has been suggested that the gating residue must move in the first step of the catalytic reaction, so as to provide access to the TPQ and to allow the TPQ to move from the "on-copper" to the "off-copper" position. In PPLO, the TPQ appears to be accessible regardless of the position of Tyr 396.

The ability of PPLO to oxidize the side chain amine groups of lysine residues in peptides and proteins is unique among the CuAOs that have been characterized so far. Further, this activity of PPLO against lysyl peptides is remarkably high. Our new data in Table 2 establish that PPLO oxidizes the side chains of tropoelastin (an in vivo substrate of mammalian lysyl oxidase) at approximately the same rate as a

Table 2: Activity of Amine Oxidases, Including *Pichia pastoris* Lysyl Oxidase, against a Recombinant Tropoelastin Substrate

enzyme	activity (dpm)[a]
control (no enzyme)	142 ± 13
bovine aorta lysyl oxidase	833 ± 52
Drosophila lysyl oxidase	813 ± 60
Pichia pastoris lysyl oxidase (PPLO)	767 ± 25
Arthrobacter globiformis amine oxidase (AGAO)	140 ± 22
pea seedling amine oxidase (PSAO)	142 ± 10
human kidney diamine oxidase	124 ± 6
equine plasma amine oxidase	134 ± 10

[a] Disintegrations per minute measuring the release of ^{3}H, as described in the methods section.

mammalian lysyl oxidase. It is remarkable that PPLO, a yeast enzyme with no sequence similarity to a mammalian lysyl oxidase, has over 90% of the activity of bovine aorta lysyl oxidase toward tropoelastin. In an assay of model hexapeptides as substrates for PPLO, the highest values of k_{cat}/K_m were recorded for peptides containing the consensus tropoelastin cross-linking sequence (*27*).

We have modeled a complex of PPLO with the substrate that had the highest activity in the comparative analysis of Tur and Lerch, namely, the hexapeptide HKHYDV (*27*) (Figure 6c,d). The PPLO funnel readily accommodates the hexapeptide substrate, and permits formation of the substrate−TPQ Schiff base complex. In general, we predict that lysine residues at or near a peptide terminus or reverse turn would be readily oxidized by PPLO. Lysine residues attached to a long helical segment, as in the triple helical domain of collagen, would be unsuitable as substrates.

REFERENCES

1. Binda, C., Mattevi, A., and Edmondson, D. E. (2002) Structure−function relationships in flavoenzyme-dependent amine oxidations: a comparison of polyamine oxidase and monoamine oxidase. *J. Biol. Chem. 277*, 23973−6.
2. Kagan, H. M. (1994) Lysyl oxidase: mechanism, regulation and relationship to liver fibrosis. *Pathol. Res. Pract. 190*, 910−9.
3. Wang, S. X., Mure, M., Medzihradszky, K. F., Burlingame, A. L., Brown, D. E., Dooley, D. M., Smith, A. J., Kagan, H. M., and Klinman, J. P. (1996) A crosslinked cofactor in lysyl oxidase: redox function for amino acid side chains. *Science 273*, 1078−84.
4. Kim, M., Okajima, T., Kishishita, S., Yoshimura, M., Kawamori, A., Tanizawa, K., and Yamaguchi, H. (2002) X-ray snapshots of quinone cofactor biogenesis in bacterial copper amine oxidase. *Nat. Struct. Biol. 9*, 591−6.
5. Tanizawa, K. (1995) Biogenesis of novel quinone coenzymes. *J. Biochem. (Tokyo) 118*, 671−8.
6. Cai, D., and Klinman, J. P. (1994) Evidence of a self-catalytic mechanism of 2,4,5-trihydroxyphenylalanine quinone biogenesis in yeast copper amine oxidase. *J. Biol. Chem. 269*, 32039−42.
7. Matsuzaki, R., Fukui, T., Sato, H., Ozaki, Y., and Tanizawa, K. (1994) Generation of the topa quinone cofactor in bacterial monoamine oxidase by cupric ion-dependent autooxidation of a specific tyrosyl residue. *FEBS Lett. 351*, 360−4.
8. Ruggiero, C. E., Smith, J. A., Tanizawa, K., and Dooley, D. M. (1997) Mechanistic studies of topa quinone biogenesis in phenylethylamine oxidase. *Biochemistry 36*, 1953−9.
9. Dooley, D. M. (1999) Structure and biogenesis of topaquinone and related cofactors. *J. Biol. Inorg. Chem. 4*, 1−11.
10. Wilmot, C. M., Hajdu, J., McPherson, M. J., Knowles, P. F., and Phillips, S. E. (1999) Visualization of dioxygen bound to copper during enzyme catalysis. *Science 286*, 1724−8.
11. Wilmot, C. M., Murray, J. M., Alton, G., Parsons, M. R., Convery, M. A., Blakeley, V., Corner, A. S., Palcic, M. M., Knowles, P. F., McPherson, M. J., and Phillips, S. E. (1997) Catalytic mechanism of the quinoenzyme amine oxidase from *Escherichia coli*: exploring the reductive half-reaction. *Biochemistry 36*, 1608−20.
12. Wilce, M. C. J., Dooley, D. M., Freeman, H. C., Guss, J. M., Matsunami, H., McIntire, W. S., Ruggiero, C. E., Tanizawa, K., and Yamaguchi, H. (1997) Crystal structures of the copper-containing amine oxidase from *Arthrobacter globiformis* in the holo- and apo-forms: implications for the biogenesis of topa quinone. *Biochemistry 36*, 16116−33.
13. Mills, S. A., and Klinman, J. P. (2000) Evidence Against Reduction of Cu2+ to Cu+ during Dioxygen Activation in a Copper Amine Oxidase from Yeast. *J. Am. Chem. Soc. 122*, 9897−904.
14. Mills, S. A., Goto, Y., Su, Q., Plastino, J., and Klinman, J. P. (2002) Mechanistic comparison of the cobalt-substituted and wild-type copper amine oxidase from *Hansenula polymorpha*. *Biochemistry 41*, 10577−84.
15. Elmore, B. O., Bollinger, J. A., and Dooley, D. M. (2002) Human kidney diamine oxidase: heterologous expression, purification, and characterization. *J. Biol. Inorg. Chem. 7*, 565−79.
16. McIntire, W. S., and Hartmann, C. (1993) Copper-containing amine oxidases in *Principles and Applications of Quinoproteins* (Davidson, V. L., Ed.) pp 97−171, Marcel Dekker, Inc, New York.
17. Sebela, M., Frebort, I., Petrivalsky, M., and Pec, P. (2002) Copper/topa quinone-containing amine oxidases − Recent research developments. *Stud. Nat. Prod. Chem. 26*, 1259−99.
18. Salmi, M., Hellman, J., and Jalkanen, S. (1998) The role of two distinct endothelial molecules, vascular adhesion protein-1 and peripheral lymph node addressin, in the binding of lymphocyte subsets to human lymph nodes. *J. Immunol. 160*, 5629−36.
19. Yu, P. H., Wright, S., Fan, E. H., Lun, Z. R., and Gubisne-Harberle, D. (2003) Physiological and pathological implications of semicarbazide-sensitive amine oxidase. *Biochim. Biophys. Acta 1647*, 193−9.
20. Parsons, M. R., Convery, M. A., Wilmot, C. M., Yadav, K. D., Blakeley, V., Corner, A. S., Phillips, S. E., McPherson, M. J., and Knowles, P. F. (1995) Crystal structure of a quinoenzyme: copper amine oxidase of *Escherichia coli* at 2 A resolution. *Structure 3*, 1171−84.
21. Kumar, V., Dooley, D. M., Freeman, H. C., Guss, J. M., Harvey, I., McGuirl, M. A., Wilce, M. C. J., and Zubak, V. M. (1996) Crystal structure of a eukaryotic (pea seedling) copper-containing amine oxidase at 2.2 Å resolution. *Structure 4*, 943−55.
22. Li, R., Klinman, J. P., and Mathews, F. S. (1998) Copper amine oxidase from *Hansenula polymorpha*: the crystal structure determined at 2.4 A resolution reveals the active conformation. *Structure 6*, 293−307.
23. Dove, J. E., and Klinman, J. P. (2001) Trihydroxyphenylalanine quinone (TPQ) from copper amine oxidases and lysyl tyrosylquinone (LTQ) from lysyl oxidase. *Adv. Prot. Chem. 58*, 141−74.
24. Dawkes, H. C., and Phillips, S. E. (2001) Copper amine oxidase: cunning cofactor and controversial copper. *Curr. Opin. Struct. Biol. 11*, 666−73.
25. Halcrow, M., Phillips, S., and Knowles, P. (2000) Amine oxidases and galactose oxidase. *Subcell. Biochem. 35*, 183−231.
26. Green, J., Haywood, G. W., and Large, P. J. (1983) Serological differences between the multiple amine oxidases of yeasts and comparison of the specificities of the purified enzymes from *Candida utilis* and *Pichia pastoris*. *Biochem. J. 211*, 481−93.
27. Tur, S. S., and Lerch, K. (1988) Unprecedented lysyloxidase activity of *Pichia pastoris* benzylamine oxidase. *FEBS Lett. 238*, 74−6.
28. Kuchar, J. A., and Dooley, D. M. (2001) Cloning, sequence analysis, and characterization of the 'Lysyl Oxidase' from *Pichia pastoris*. *J. Inorg. Biochem. 83*, 193−204.
29. Dove, J. E., Smith, A. J., Kuchar, J., Brown, D. E., Dooley, D. M., and Klinman, J. P. (1996) Identification of the quinone cofactor in a lysyl oxidase from *Pichia pastoris*. *FEBS Lett. 398*, 231−4.
30. Lee, M., Willingham, K., Langley, D., Maher, M. J., Cohen, A. E., Ellis, P. J., Kuchar, J. A., Dooley, D. M., Freeman, H. C., and Guss, J. M. (2002) Crystallization of *Pichia pastoris* lysyl oxidase. *Acta Crystallogr. D58*, 2177−9.
31. Navaza, J. (1994) AMoRe: an Automated Package for Molecular Replacement. *Acta Crystallogr. D55*, 157−63.
32. Matthews, B. W. (1968) Solvent Content of Protein Crystals. *J. Mol. Biol. 33*, 491−7.

33. Altschul, S. F., Gish, W., Miller, W., Myers, E. W., and Lipman, D. J. (1990) Basic local alignment search tool. *J. Mol. Biol. 215*, 403−10.
34. Brunger, A. T., Adams, P. D., Clore, G. M., Delano, W. L., Gros, P., Grossekunstleve, R. W., Jiang, J. S., Kuszewski, J., Nilges, M., Pannu, N. S., Read, R. J., Rice, L. M., Simonson, T., and Warren, G. L. (1998) Crystallography and NMR system − a new software suite for macromolecular structure determination. *Acta Crystallogr. D54*, 905−21.
35. Jones, T. A., Zou, J.-Y., Cowan, S. W., and Kjeldgaard, M. (1991) Improved methods for building protein models in electron density maps and the location of errors in these models. *Acta Crystallogr. A47*, 110−9.
36. Cowtan, K. (1994) An automated procedure for phase improvement by density modification, *Joint CCP4 and ESF-EACBM Newsletter on Protein Crystallography 31*, 34−8.
37. Perrakis, A., Harkiolaki, M., Wilson, K. S., and Lamzin, V. S. (2001) ARP/wARP and molecular replacement. *Acta Crystallogr. D57*, 1445−50.
38. Murshudov, G. N., Vagin, A. A., and Dodson, E. J. (1997) Refinement of macromolecular structures by the maximum-likelihood method. *Acta Crystallogr. D53*, 240−55.
39. CCP4. (1994) Collaborative Computational Project no. 4, *Acta Crystallogr. D50*, 760−3.
40. Bedell-Hogan, D., Trackman, P., Abrams, W., Rosenbloom, J., and Kagan, H. (1993) Oxidation, cross-linking, and insolubilization of recombinant tropoelastin by purified lysyl oxidase. *J. Biol. Chem. 268*, 10345−50.
41. Kuchar, J. A. (2001) Cloning, sequence analysis, and characterization of the 'lysyl oxidase' from *Pichia pastoris*, Ph.D. Thesis, Montana State University.
42. Kagan, H. M., and Cai, P. (1995) Isolation of active site peptides of lysyl oxidase. *Methods Enzymol. 258*, 122−32.
43. Kleywegt, G. J., and Jones, T. A. (1994) Detection, Delineation, Measurement and Display of Cavities in Macromolecular Structures. *Acta Crystallogr. D50*, 178−85.
44. Delano, W. L. (2002) Delano Scientific, San Carlos, CA.
45. Cruickshank, D. W. J. (1999) Remarks about protein structure precision. *Acta Crystallogr. D55*, 583−601.

BI035338V